Geophysical Research Letters

Supporting Information for

Spatially resolved photochemistry impacts emissions estimates in fresh wildfire plumes

Brett B. Palm[1,*,#], Qiaoyun Peng[1], Samuel R. Hall[2], Kirk Ullmann[2], Teresa L. Campos[2], Andrew Weinheimer[2], Deedee Montzka[2], Geoffrey Tyndall[2], Wade Permar[3], Lu Hu[3], Frank Flocke[2], Emily V. Fischer[4], Joel A. Thornton[1]

[1]Department of Atmospheric Sciences, University of Washington, Seattle, WA, USA 98195

[2]Atmospheric Chemistry Observations and Modeling Laboratory, National Center for Atmospheric Research, Boulder, CO, USA 80301

[3]Department of Chemistry and Biochemistry, University of Montana, Missoula, MT, USA 59812

[4]Department of Atmospheric Science, Colorado State University, Fort Collins, CO, USA 80523

[@]Now at: Atmospheric Chemistry Observations and Modeling Laboratory, National Center for Atmospheric Research, Boulder, CO, USA 80301

[#]Corresponding author: Brett B. Palm (bbpalm@ucar.edu)

Contents of this file

S1 Instrument and measurement details

The I^- CIMS measured a variety of organic and inorganic compounds, including HONO, HCN, several likely phenolic compounds, and a suite of other oxidized organic compounds. Ambient air was sampled at 20 lpm through a ¾" OD, ~50 cm long PTFE Teflon tube into the cabin. Air was then subsampled at 2 slpm into the CIMS through a custom inlet (Palm et al., 2019). Data was collected at 2 Hz and averaged to 1 Hz for use. The calibration factors used for each compound are described in Palm et al. (2020). $C_3H_4O_3$ was not calibrated due to a lack of knowledge of the sampled isomer composition, so mixing ratios were calculated using a typical calibration value of 5 counts per second per million reagent ions per pptv. $C_6H_6O_2$ was screened to remove measurement "tails" that result from that compound interacting with inlet surfaces (see Palm et al., 2019), by removing any $C_6H_6O_2$ data where $C_6H_6O_1$ (a compound with minimal inlet surface interactions) had decayed to below 20% of its peak in each transect. The other I^- CIMS compounds used here are more volatile and thus did not have such inlet artifacts.

CO was sampled using a commercial Mini-QCL tunable diode laser infrared absorption spectrometer (Lebegue et al., 2016). To optimize measurement accuracy, the spectrometer optical bench was continuously purged with synthetic zero grade air from which CO had been scrubbed to contain less than 1 ppbv. N_2O was also measured by the Mini-QCL, and was quantified in the purge gas at typically less than 0.3 ppbv. The N_2O purge gas concentration was included in spectral fit calculations to better reproduce the spectral background. The CO measurement had a precision of 0.1 ppbv with a 2 s temporal resolution and an accuracy of +/- 0.6 ppbv. The photolysis rate of HONO (j_{HONO}) was calculated from actinic flux measurements taken by the HIAPER Atmospheric Radiation Package (HARP; Shetter & Müller, 1999). Ozone (O_3) was measured by a chemiluminescense instrument at 1 Hz, with an accuracy of 5%. A proton transfer reaction time-of-flight mass spectrometer (PTR-ToF-MS) was used to measure a suite of volatile organic compounds (VOCs), including C_6H_6 and C_7H_8 used here (Permar et al., 2021). The data from various instruments were aligned in time by maximizing correlations of non-reactive compounds in the plumes.

The physical age of each transect was estimated by dividing the average distance from each transect to the fire source location by the average wind speed measured in the plume. The solar zenith angle (SZA) at time of emission (sampled time minus physical age) was calculated for each sampled latitude and longitude using the NOAA Solar Calculator, based on equations from *Astronomical Algorithms*, by Jean Meeus.

NEMRs were calculated as background-subtracted ratios of various compounds to CO. The background values were determined by averaging out-of-plume measurements from before and/or after each transect (typically 15 s on each side) to get a single background value per transect for each compound. Some transects did not fully exit the plume, so their background values were determined using data from only one side of the transect. Such transects were identified by comparing with the backgrounds determined in nearby transects and looking for outliers. While the South Sugarloaf fire was confined to (and diluted with) the boundary layer, the airplane occasionally transitioned into free tropospheric air while sampling the background before or after some transects sampled at the very top of the plume. Free tropospheric air was

identified by, e.g., low mixing ratios of water vapor, formic acid, and a variety of other compounds. This air was not representative of the air with which the plume was diluting, so such measurements were not included as background values. The Taylor Creek Fire plume, on the other hand, was injected into (and predominantly diluted with) the free troposphere, so background values were selected from free tropospheric air before and after each transect.

S2 Methodology for estimating $[OH]_{avg}$ in the Taylor Creek Fire plume

In non-diluting systems, e.g., batch chamber experiments of photochemical aging, OH concentrations can be derived by measuring the decay of a single compound and applying reaction kinetics. In diluting systems, e.g., urban downwind or wildfire plumes, the photochemical aging can be spatially inhomogeneous and difficult to estimate because of dilution and variations in parameters such as actinic flux. Previous studies of urban plumes have estimated photochemical age at various locations downwind by analyzing the change in the ratio of two compounds with a known emission ratio (de Gouw et al., 2005; Roberts et al., 1984). Dilution acts equally on the concentration of both compounds, so a change in the ratio indicates oxidation chemistry (or other formation/loss processes) when the two compounds have different reactivities. For systems where physical age can be estimated (e.g., wildfire or other point sources), the photochemical age estimated from changing ratios can be converted to average oxidant concentrations.

Past studies of urban air have used various organic compounds but not CO (de Gouw et al., 2005; Roberts et al., 1984), because CO is emitted by many urban sources at different rates. For wildfires, CO emissions can be characterized directly with measurements for individual fires, so it can be used as one of the two compounds.

To estimate the fractional fate of $C_6H_6O_2$ to reaction with OH, NO_3, or O_3 in the Taylor Creek Fire plume, we used the Framework for 0-D Atmospheric Modeling (F0AM) box model with the Master Chemical Mechanism (MCM) v3.3.1 chemical mechanism (Jenkin et al., 2015; Wolfe et al., 2016). The MCM is a near-explicit chemical mechanism with detailed gas-phase chemical processes for a variety of compounds, including 142 primarily emitted non-methane VOCs and their oxidation products. Additional mechanisms were added, including the recent mechanism development from laboratory measurements for heterocyclic hydrocarbons (like furans) and phenolics, which are found to significantly contribute to secondary product formation in biomass burning plumes (Coggon et al., 2019; Decker et al., 2019; Joo et al., 2019).

In Fig. S3, we show the fractional loss of $C_6H_6O_2$ to each of the oxidants when initializing the model with mixing ratios measured in the core (95^{th} percentile [CO]) or the edges (30^{th} percentile [CO]) of the plume. We estimate that 28% of $C_6H_6O_2$ will react with NO_3 in the core, and 10% on the edges. O_3 accounts for a negligible several percent, with the remainder going to reaction with OH. When estimating the fractional fates across the entire plume for the purposes of estimating $[OH]_{avg}$ in Sect. 3.1.2, we assumed 75% of $C_6H_6O_2$ reacted with OH in the Taylor Creek plume. The uncertainties associated with this assumption are likely small relative to those in the sensitivity analysis of the initial $C_6H_6O_2$ to CO ratio in Sect S3. This analysis also suggests that reaction with OH, not with NO_3, was the cause of the measured

crosswind gradients, since NO_3 was found to account for less reaction on the edges versus the plume core.

S3 Sensitivity analysis

Since it was not possible to sample the exact emission ratios of highly reactive compounds such as $C_6H_6O_2$ in authentic wildfires from the aircraft platform, the initial ratio of $C_6H_6O_2$ to CO is a source of uncertainty. In Sect. 3.1.2, we used an initial ratio of 1. The evolution of this ratio with plume age is shown in Fig. S6b. In Fig. S5, we show the calculations of $[OH]_{avg}$ using initial ratios of 0.7 and 1.5 to show the sensitivity of this calculation to the initial ratio. The estimated $[OH]_{avg}$ in the freshest transects varies by up to approximately a factor of two, but the gradients are robust. The $[OH]_{avg}$ in aged transects is less sensitive to the initial ratio. We also investigated the use of different compound ratios, including $C_6H_6O_1$ to CO, $C_6H_6O_2$ to $C_6H_6O_1$, and C_7H_8 to C_6H_6 as shown in Fig. S6. None of the compounds except $C_6H_6O_2$ were expected to react appreciably with oxidants other than OH. The results were similar, with the exception that the fresh plume gradients were not as clear when $C_6H_6O_2$ is not one of the compounds used. The likely reason for this behavior is that $C_6H_6O_2$ is the only compound that reacts with OH fast enough to form measureable gradients on this time scale. After an estimated 22 min of physical age in the freshest transects, the fraction of $C_6H_6O_2$ remaining for $[OH]_{avg}$ values of 1.0×10^7 and 4×10^6 molecules cm^{-3} (plume edges versus core) is expected to be 30% and 62%, which is a measurable difference in the freshest crosswind transects. For $C_6H_6O_1$, we expect 73% and 88% remaining, which is similar to the expected measurement precision and other possible uncertainties (e.g., any variable emissions between core and edge). For C_7H_8, 94% and 97% are expected, which are indistinguishable in a single crosswind transect to within uncertainties, and C_6H_6 is even less reactive. Therefore, $C_6H_6O_2$ was the best available compound for calculating $[OH]_{avg}$ in the highly reactive and fresh Taylor Creek plume, and compounds such as C_7H_8 and C_6H_6 are not suitable for quantifying gradients on such short time scales.

S4 Additional vertically stacked transects in the South Sugarloaf fire

Several other vertically stacked transects of the South Sugarloaf fire plume were conducted in addition to those in Sect. 3.2. In Fig. S10, the upper two crosswind transects through the plume sampled at an age of 47 min from 1415-1445 LT clearly show steep vertical gradients in HONO, $C_6H_6O_2$, and O_3 at the top of the plume. The uppermost transect appears to have skimmed close to the top of the plume, where photolysis rates were much higher than the other transect ~350 m lower. In Fig. S11, a stack of transects at the same 47 min age but sampled as the sun was setting at 1850-1925 LT illustrates how the observed gradients were changing as day became night. The j_{HONO} values were low even outside of the plume, and the gradients in reactive compounds such as HONO and $C_6H_6O_2$ were much smaller, indicating OH production and associated chemistry were greatly slowed. In fact, O_3 was depleted in all locations inside the plume relative to background air in these evening transects, but especially in the denser portion of the plume at higher altitudes. Fig. S11 illustrates the behavior that is likely to be observed in wildfire plumes that are emitted at/after sunset. The differences in observed gradients highlights the need to understand the different chemical and physical evolution of daytime and nighttime plumes to model the downwind effects of emissions occurring throughout the day and night.

Figure S1. Images from the forward facing camera on the C-130 aircraft showing how the Taylor Creek Fire plume injected above the smoke-filled boundary layer into the free troposphere. The image on the left shows the plume shortly after injection, and the image on the right shows the evolution of the plume approximately 90 minutes later.

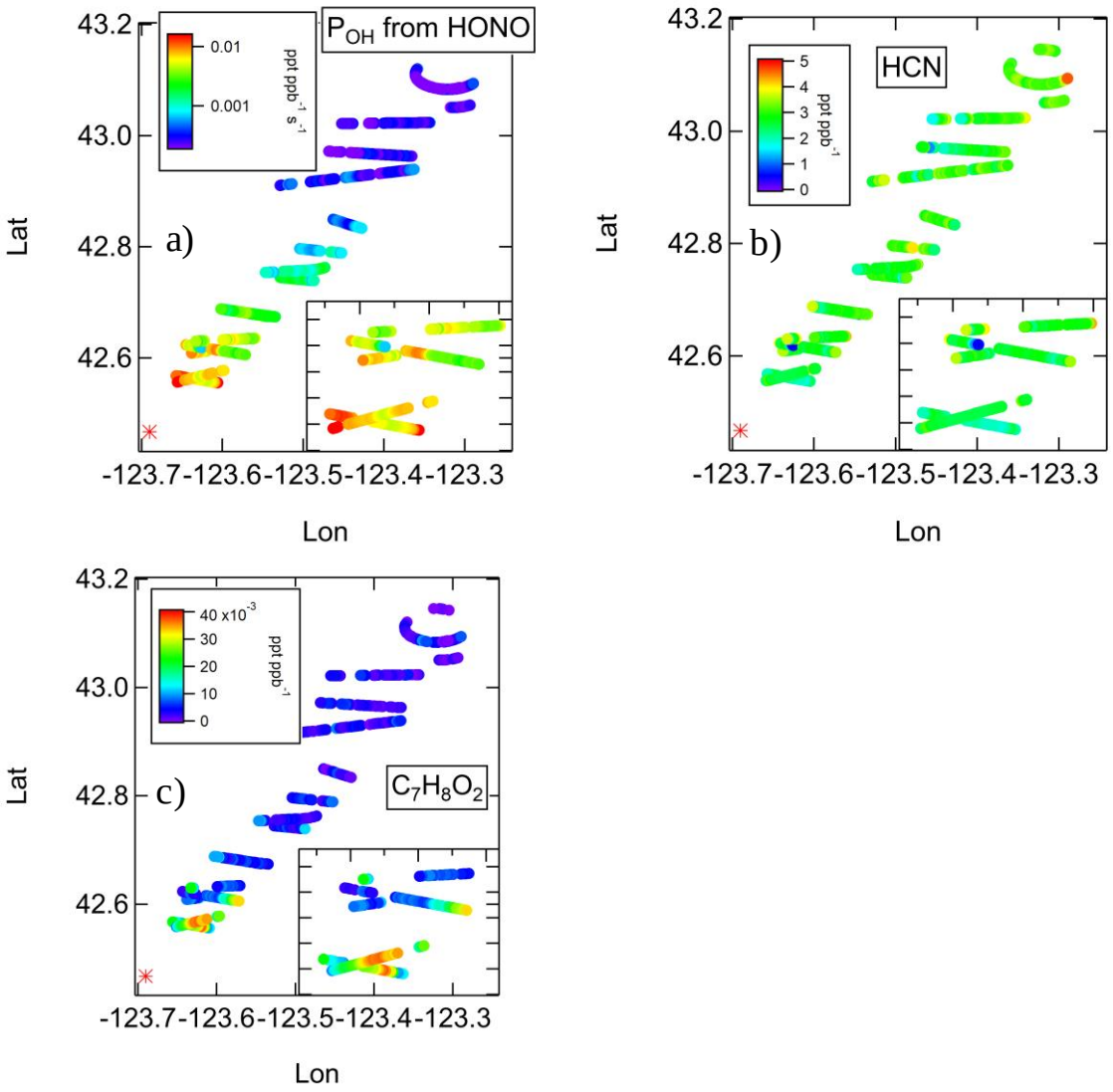

Figure S2. Plume transects in the Taylor Creek fire, showing spatial variations in a) the dilution-corrected production rate of OH from HONO photolysis, and the NEMRs of b) HCN and c) $C_7H_8O_2$. The insets show the first five transects in greater detail. Gradients were not observed for HCN, in contrast to the NEMRs of reactive compounds shown in Fig. 1.

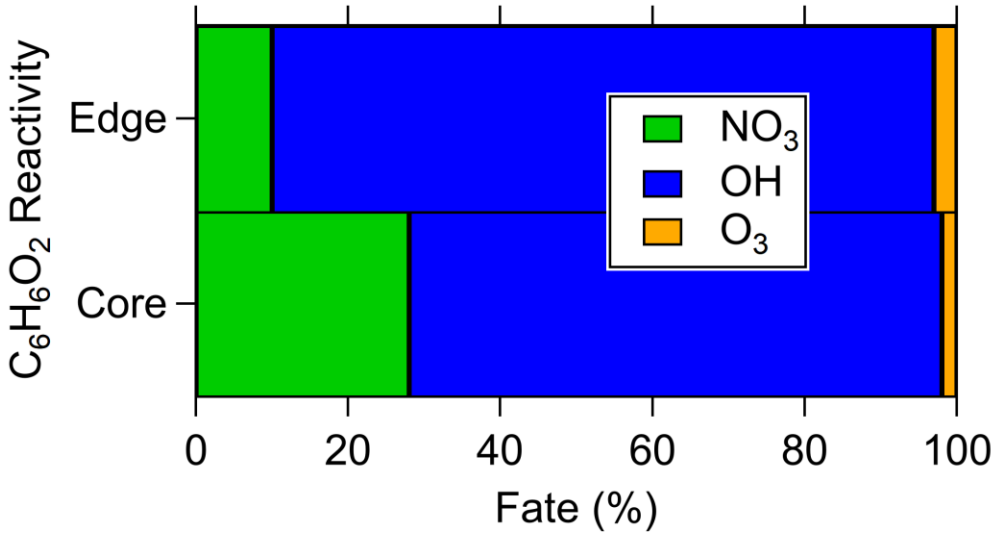

Figure S3. Percentage of reactivity of $C_6H_6O_2$ to oxidants in the Taylor Creek Fire plume. The reactivity was modeled using the F0AM box model when initializing the model with mixing ratios measured in the plume core (95th percentile [CO]) or on the plume edges (30th percentile values).

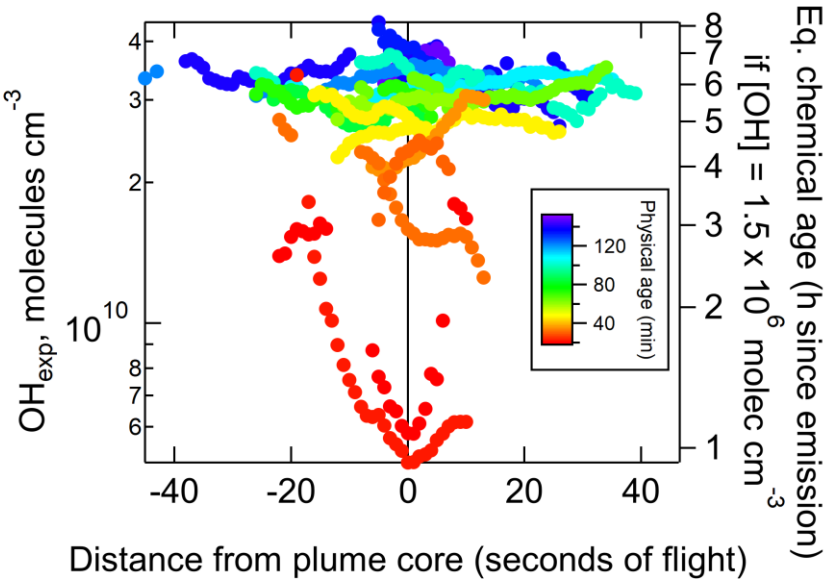

Figure S4. OH_{exp} at each sampled location in the Taylor Creek Fire plume, as a function of distance from the plume core. Data are colored by estimated physical age.

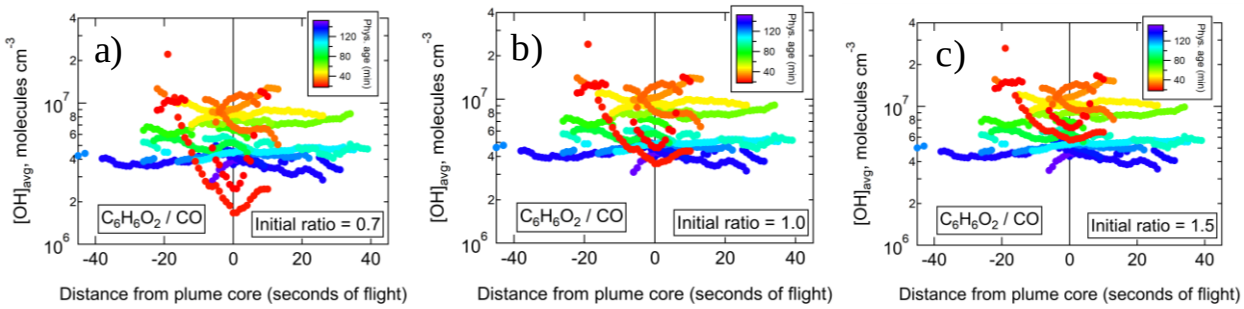

Figure S5. Calculations of $[OH]_{avg}$ in the Taylor Creek plume using initial $C_6H_6O_2$ to CO ratios of a) 0.7, b) 1, same as Fig. 2b, and c) 1.5. Data are colored by estimated physical age. This sensitivity analysis illustrates the absolute magnitude of $[OH]_{avg}$ varies by up to a factor of two over this range of initial ratios, but the existence of crosswind gradients and the evolution with plume age is robust.

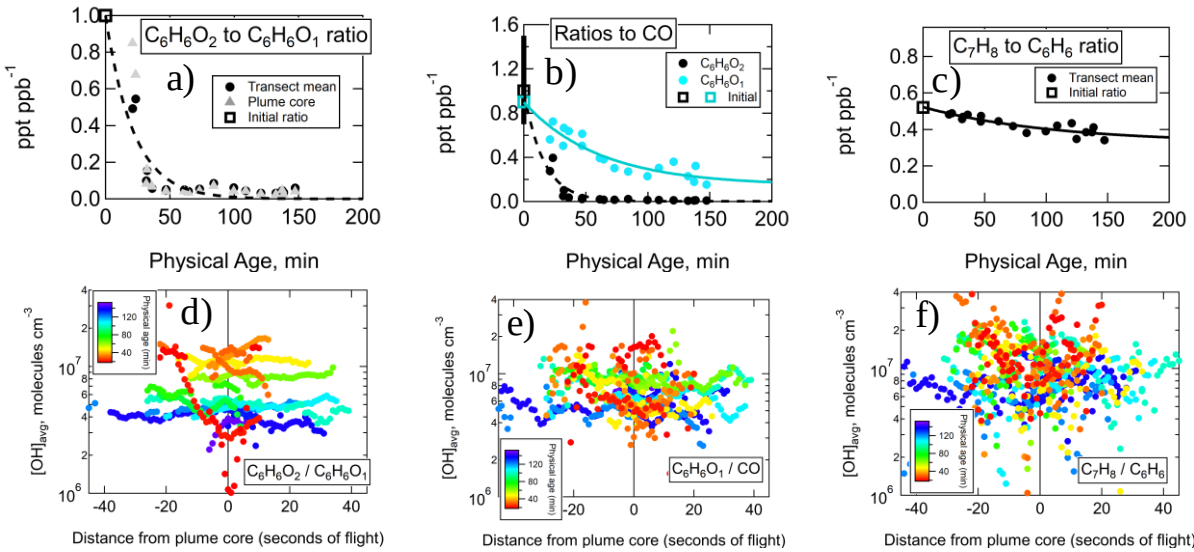

Figure S6. a, b, and c) The derivation of initial ratios, and d, e, and f) calculations of $[OH]_{avg}$ in the Taylor Creek plume using different compound ratios, for comparison to Fig. 2. See Sect. S3 for discussion.

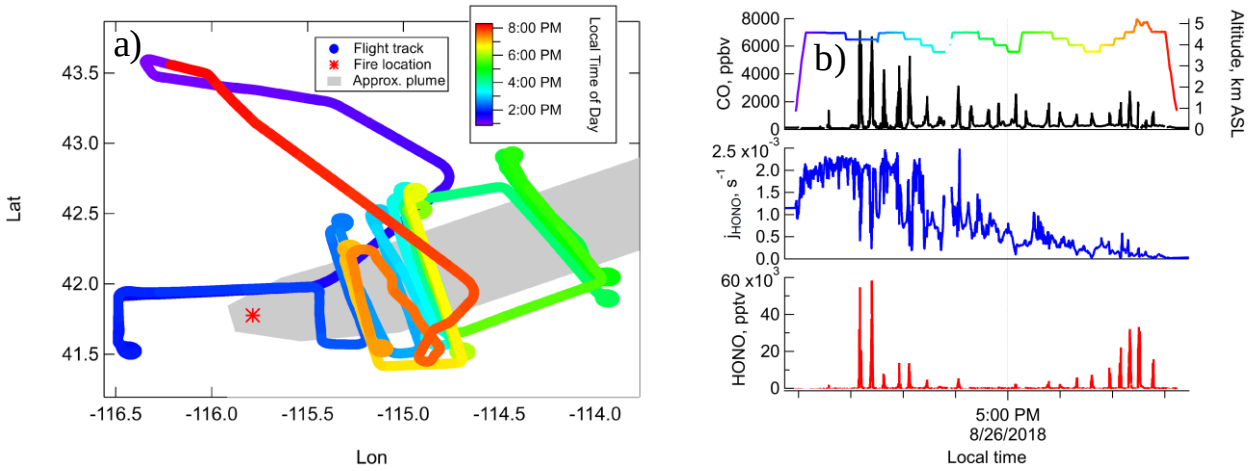

Figure S7. a) Flight track for the South Sugarloaf fire on Aug. 26, 2018, colored by local time of day and showing approximate fire and plume locations, and b) measurements of altitude, CO, j_{HONO}, and HONO, illustrating the changing photochemical conditions during the time of plume sampling. Altitude is also colored by local time of day.

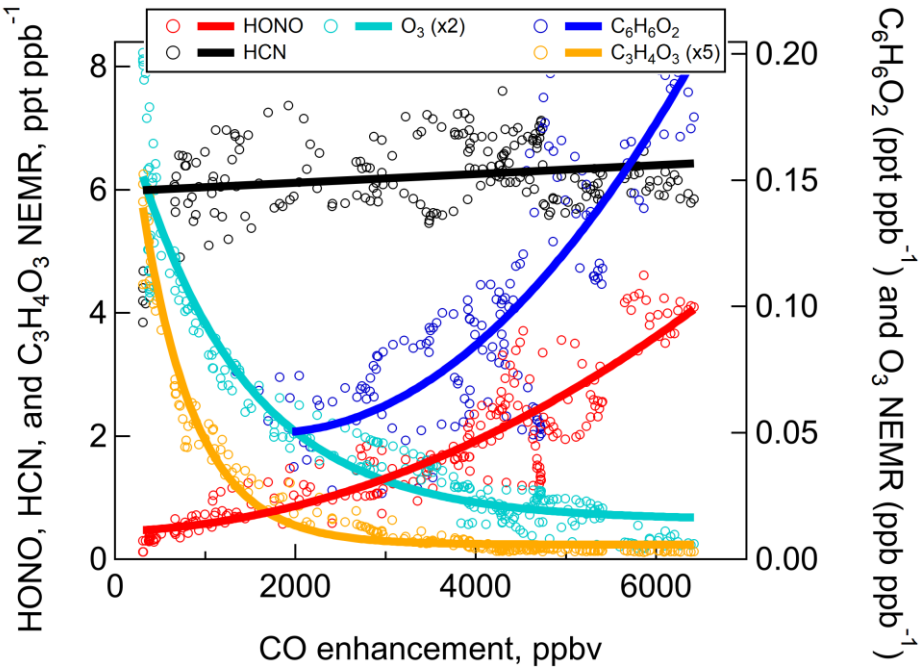

Figure S8. Gradients in several compounds as a function of CO enhancement above background in a crosswind transect of the South Sugarloaf fire plume. The highest CO enhancements are near the dark plume center, and CO enhancement decreases due to dilution on plume edges. This transect was sampled at an est. physical age of 44 min at 1420 LT. Reactive compounds such as HONO and $C_6H_6O_2$ are depleted on plume edges relative to center, due to faster photochemistry. Similarly, oxidation products such as O_3 and $C_3H_4O_3$ are enhanced on plume edges relative to center. Not all plume transects have the prototypical Gaussian shape, so plotting as a function of CO enhancement instead of distance from plume center (defined by highest CO) can be useful.

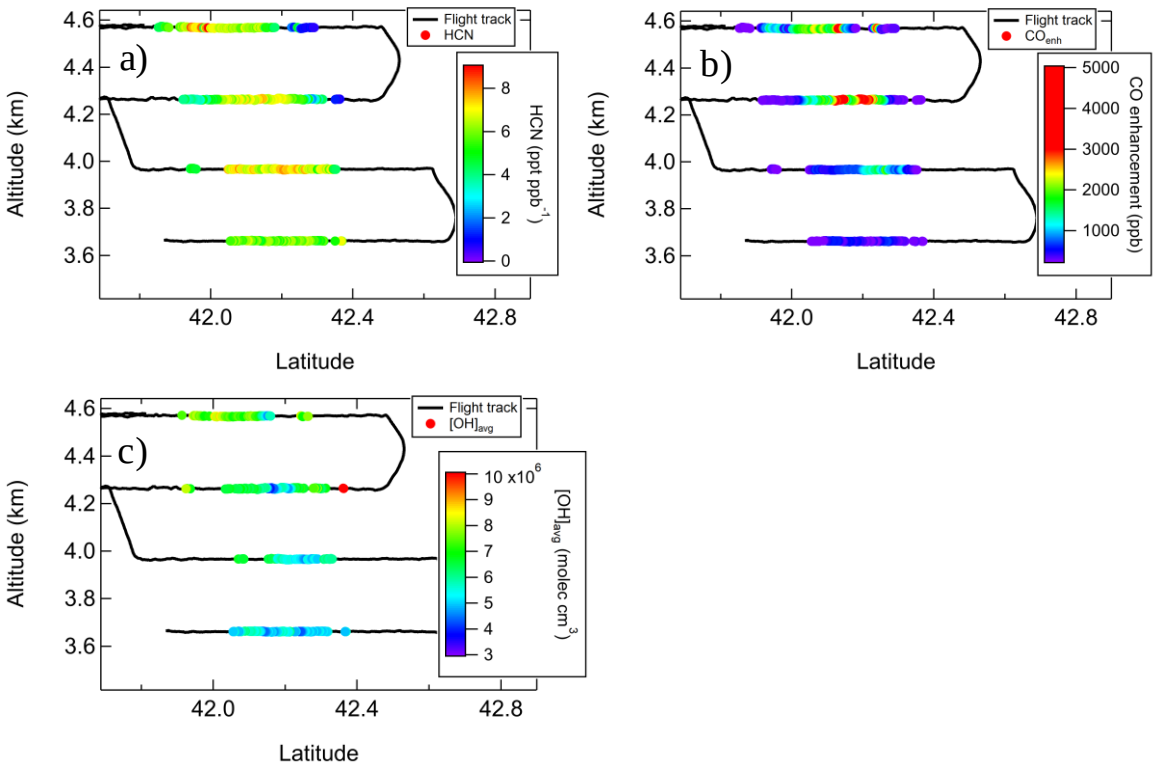

Figure S9. For comparison with Fig. 3, a) HCN, b) CO enhancement, and c) $[OH]_{avg}$ in four vertically stacked transects of the South Sugarloaf fire, sampled at an average est. physical age of 76 min from 1450-1550 LT. Relatively nonreactive compounds such as HCN remain roughly constant throughout each transect.

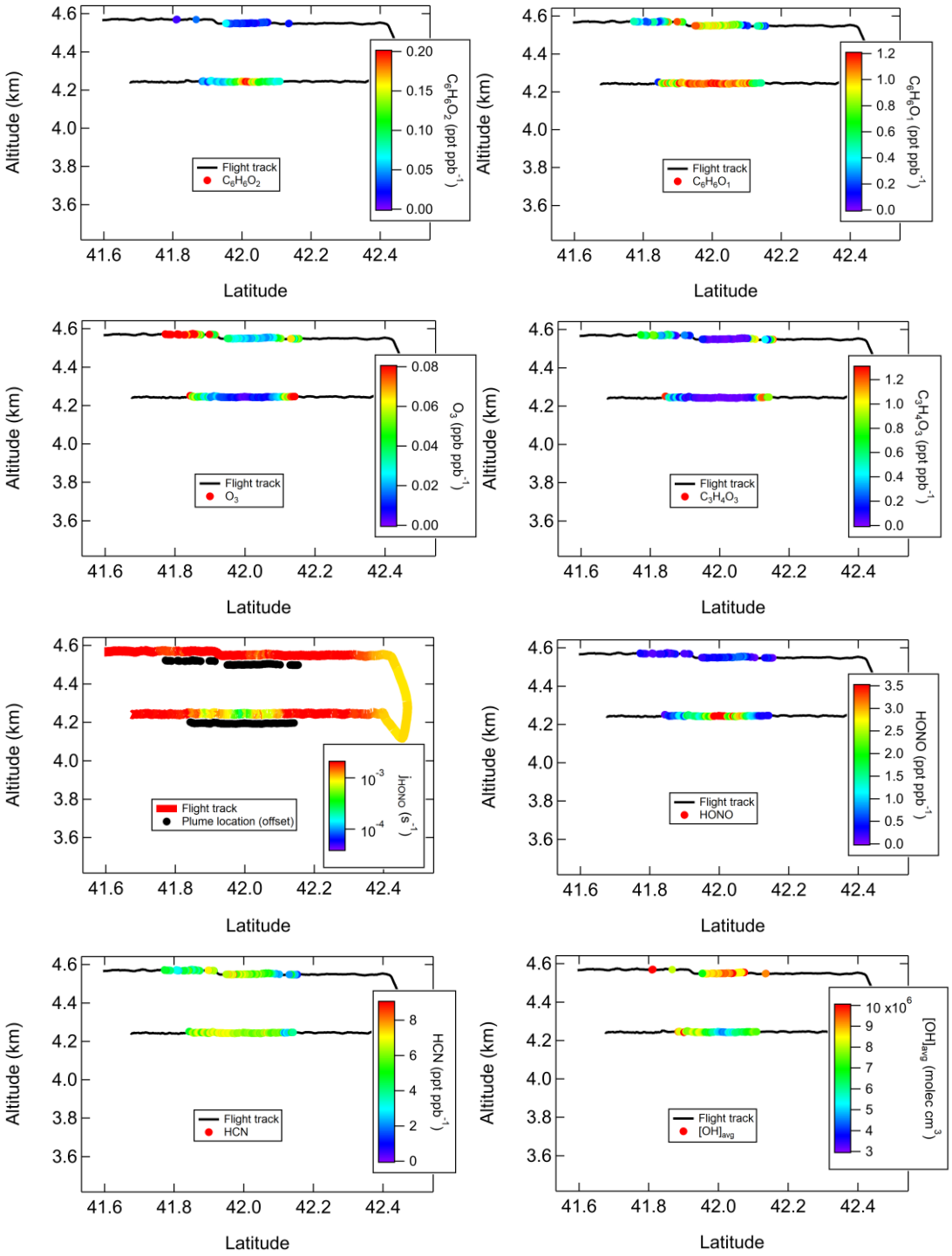

Figure S10. Various measurements in two vertically stacked transects in the South Sugarloaf fire sampled at an average physical age of 47 min, sampled from 1415-1445 LT. The upper transect had higher photolysis rates, leading to faster O_3 formation with more depleted HONO and $C_6H_6O_2$. This figure can be compared with Fig. S11, which shows a similar estimated physical age but sampled late in the day with different chemical conditions leading to weaker gradients.

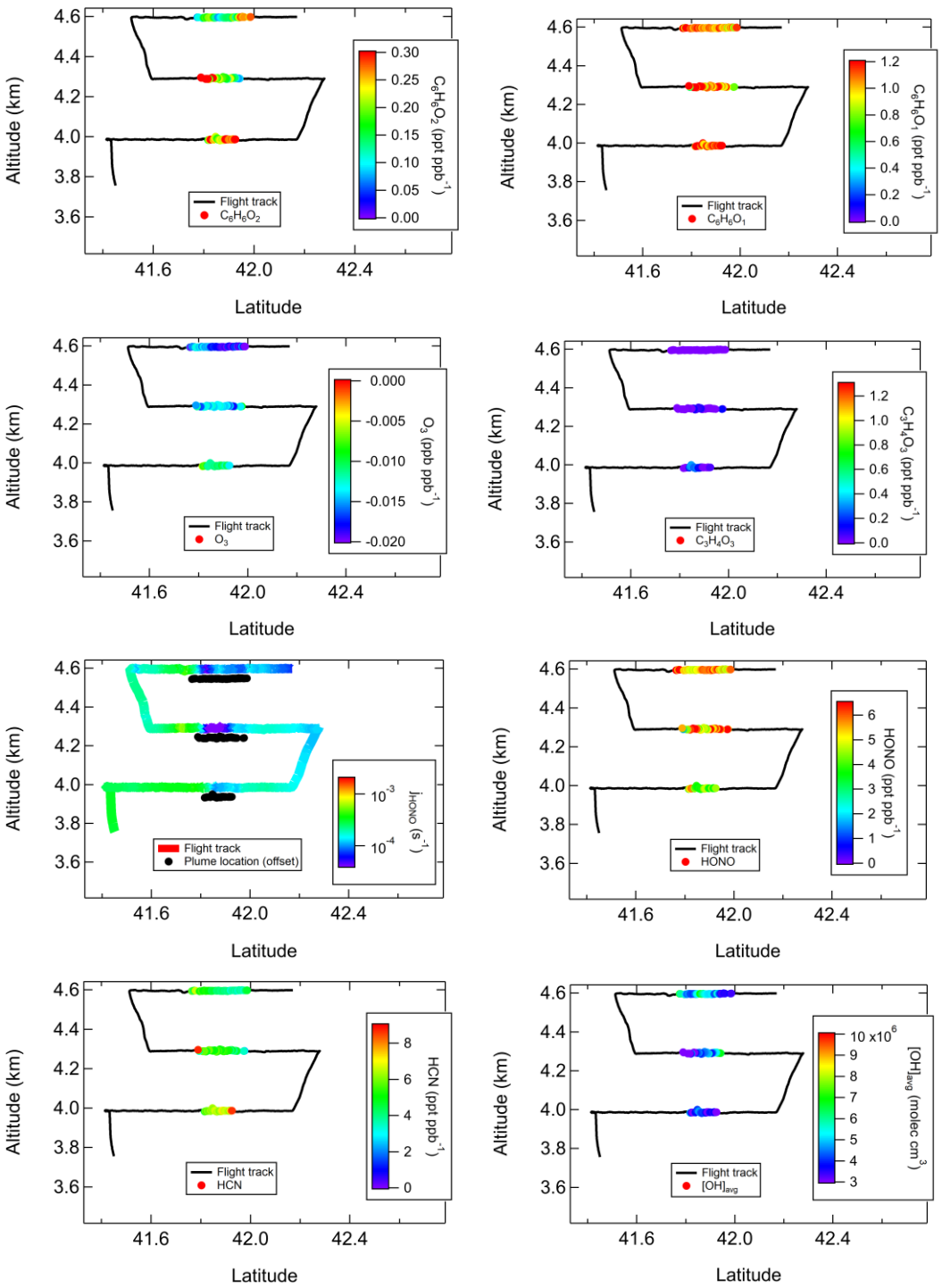

Figure S11. Various measurements in three vertically stacked transects at an estimated physical age of 47 min, sampled from 1850-1925 LT, close to sunset. O_3 is depleted relative to the background. HONO and $C_6H_6O_2$ remain in relatively high abundances across the plume transects, illustrating slower photochemistry leading to lesser gradients. This figure can be compared with Fig. S10, which shows a similar estimated physical age but sampled in the middle of daytime with more rapid chemistry and stronger gradients.

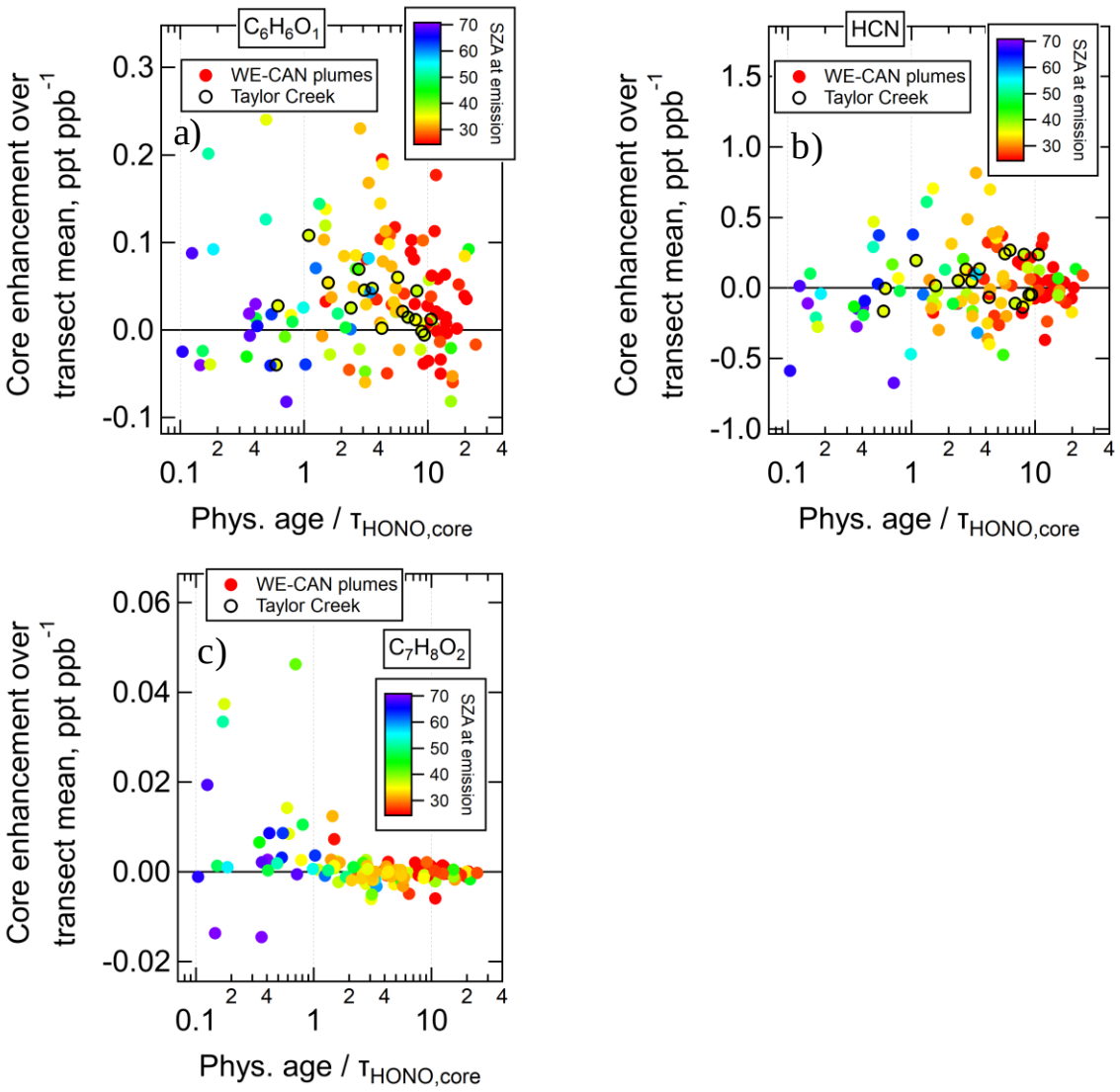

Figure S12. Enhancements of NEMRs in plume cores (average where [CO] > 90th percentile) relative to transect mean NEMRs for all WE-CAN transects, for a) $C_6H_6O_1$, b) HCN, and c) $C_7H_8O_2$ (methyl catechol; see Palm et al., 2020) for comparison with Fig. 4. The Taylor Creek plume transects are highlighted.

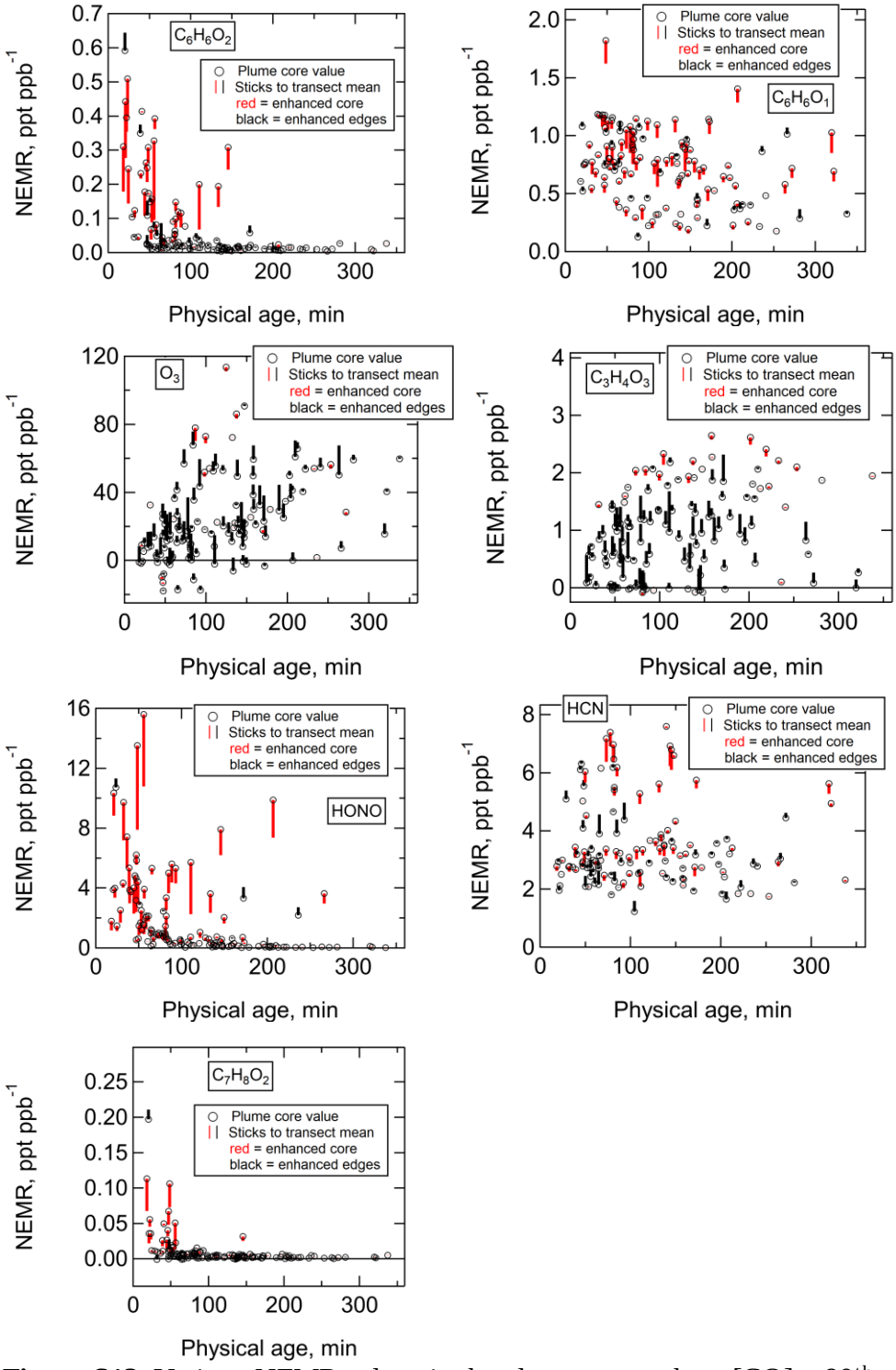

Figure S13. Various NEMR values in the plume cores where [CO] > 90th percentile (open circles), relative to transect mean NEMRs (other end of sticks). Sticks are red when the core is higher than the transect mean, and black when the core value is lower. Reactive emissions are generally enhanced in the core, oxidation products are enhanced on the edges, and unreactive compounds such as HCN show little gradients.

Table S1. Rate constants for reactions of OH with various compounds used in this analysis.

Molecular formula	Compound	k_{OH} rate constant (cm^3 $molecule^{-1}$ s^{-1})
$C_6H_6O_1$	Phenol	2.6×10^{-11} ([1])
$C_6H_6O_2$	Catechol	1.0×10^{-10} ([2])
C_7H_8	Toluene	5.6×10^{-12} ([3])
C_6H_6	Benzene	1.2×10^{-12} ([3])
CO	Carbon monoxide	2.4×10^{-13} ([4])

[1](Atkinson et al., 1989)
[2](Olariu et al., 2000)
[3](Atkinson & Arey, 2003)
[4](Burkholder et al., 2019)